



# Studies on Inhibition of Respiratory Cytochrome $bc_1$ Complex by the Fungicide Pyrimorph Suggest a Novel Inhibitory Mechanism

Yu-Mei Xiao<sup>1,2</sup>, Lothar Esser<sup>2</sup>, Fei Zhou<sup>2</sup>, Chang Li<sup>1</sup>, Yi-Hui Zhou<sup>1,2</sup>, Chang-An Yu<sup>3</sup>, Zhao-Hai Qin<sup>1\*</sup>, Di Xia<sup>2\*</sup>

**1** Department of Applied Chemistry, China Agricultural University, Beijing, China, **2** Laboratory of Cell Biology, Center for Cancer Research, National Cancer Institute, NIH, Bethesda, Maryland, United States of America, **3** Department of Biochemistry and Molecular Biology, Oklahoma State University, Stillwater, Oklahoma, United States of America

## Abstract

The respiratory chain cytochrome  $bc_1$  complex (cyt  $bc_1$ ) is a major target of numerous antibiotics and fungicides. All cyt  $bc_1$  inhibitors act on either the ubiquinol oxidation ( $Q_P$ ) or ubiquinone reduction ( $Q_N$ ) site. The primary cause of resistance to  $bc_1$  inhibitors is target site mutations, creating a need for novel agents that act on alternative sites within the cyt  $bc_1$  to overcome resistance. Pyrimorph, a synthetic fungicide, inhibits the growth of a broad range of plant pathogenic fungi, though little is known concerning its mechanism of action. In this study, using isolated mitochondria from pathogenic fungus *Phytophthora capsici*, we show that pyrimorph blocks mitochondrial electron transport by affecting the function of cyt  $bc_1$ . Indeed, pyrimorph inhibits the activities of both purified 11-subunit mitochondrial and 4-subunit bacterial  $bc_1$  with  $IC_{50}$  values of 85.0  $\mu$ M and 69.2  $\mu$ M, respectively, indicating that it targets the essential subunits of cyt  $bc_1$  complexes. Using an array of biochemical and spectral methods, we show that pyrimorph acts on an area near the  $Q_P$  site and falls into the category of a mixed-type, noncompetitive inhibitor with respect to the substrate ubiquinol. *In silico* molecular docking of pyrimorph to cyt  $b$  from mammalian and bacterial sources also suggests that pyrimorph binds in the vicinity of the quinol oxidation site.

**Citation:** Xiao Y-M, Esser L, Zhou F, Li C, Zhou Y-H, et al. (2014) Studies on Inhibition of Respiratory Cytochrome  $bc_1$  Complex by the Fungicide Pyrimorph Suggest a Novel Inhibitory Mechanism. PLoS ONE 9(4): e93765. doi:10.1371/journal.pone.0093765

**Editor:** Lijun Rong, University of Illinois at Chicago, United States of America

**Received:** February 20, 2014; **Accepted:** March 5, 2014; **Published:** April 3, 2014

This is an open-access article, free of all copyright, and may be freely reproduced, distributed, transmitted, modified, built upon, or otherwise used by anyone for any lawful purpose. The work is made available under the Creative Commons CC0 public domain dedication.

**Funding:** This research was supported in part by the Intramural Research Program of the NIH, National Cancer Institute, Center for Cancer Research, and by a grant from the National Basic Research Science Foundation of China (2010CB126100) to ZQ. The funders had no role in study design, data collection and analysis, decision to publish, or preparation of the manuscript.

**Competing Interests:** The authors have the following interests. Dimethomorph was a gift from Jiangshu Frey Chemical Co. Ltd. (Jiangshu Province, China). This does not alter the authors' adherence to all the PLOS ONE policies on sharing data and materials, as detailed online in the guide for authors.

\* E-mail: qinzhaochai@263.net (ZQ); xiad@mail.nih.gov (DX)

## Introduction

The cytochrome  $bc_1$  complex (cyt  $bc_1$ , also known as ubiquinone:cyt  $c$  oxidoreductase, Complex III or  $bc_1$ ) is a central component of the cellular respiratory chain of mitochondria. It catalyzes the reaction of electron transfer (ET) from ubiquinol to cyt  $c$  and couples this reaction to proton translocation across the mitochondrial inner membrane, contributing to the cross-membrane proton motive force essential for cellular functions such as ATP synthesis [1,2]. The indispensable function of cyt  $bc_1$  in cellular energy metabolism makes it a prime target for numerous natural and synthetic antibiotics. More than 20 synthetic fungicides targeting cyt  $bc_1$  are in widespread use in agriculture with an annual sale exceeding \$2.7 billion [3].

All cyt  $bc_1$  inhibitors target either the ubiquinol oxidation site ( $Q_P$  or  $Q_O$ ) or the ubiquinone reduction site ( $Q_N$  or  $Q_I$ ), which are defined by the Q-cycle mechanism of cyt  $bc_1$  function [4,5]. Despite variations in subunit compositions of  $bc_1$  from various organisms, only three subunits are essential for ET-coupled proton translocation function: they are cyt  $b$ , cyt  $c_1$  and the iron-sulfur protein (ISP). The cyt  $b$  subunit contains two  $b$ -type hemes ( $b_L$  and  $b_H$ ), the cyt  $c_1$  subunit has a  $c$ -type heme, and the ISP possesses a

2Fe-2S cluster. Both active sites are located within the cyt  $b$  subunit, as demonstrated by crystallographic studies of mitochondrial and bacterial  $bc_1$  complexes [6–12]. Resistance to known cyt  $bc_1$  fungicides has been reported at an alarming rate, rendering many of these reagents ineffective. Most common mechanisms of resistance involve target site mutations and corresponding strategies to overcome drug resistance have been proposed [13]. Developing new agents targeting areas outside the  $Q_P$  and  $Q_N$  sites of cyt  $bc_1$  is most attractive primarily because the new compounds presumably are able to circumvent existing fungal resistance.

Pyrimorph, (Z)-3-[(2-chloropyridine-4-yl)-3-(4-*tert*-butylphenyl)-acryloyl] morpholine, is a novel systemic antifungal agent that belongs to the family of carboxylic acid amide (CAA) fungicides [14], whose members include mandipropamid, dimethomorph, flumorph, and valinine derivatives. Pyrimorph exhibits excellent activity inhibiting mycelial growth of the fungal species *Phytophthora infestans*, *Phytophthora capsici*, and *Rhizoctonia solani* and is able to suppress zoospore germination of *Pseudoperonospora cubensis* with  $EC_{50}$  values in the range between 1.3 and 13.5  $\mu$ M [15]. The *in vitro* sensitivities of various asexual stages of *Peronospora litchii*

to pyrimorph were studied with four single-sporangium isolates, showing high sensitivity at the stage of mycelial growth with an EC<sub>50</sub> of 0.3 μM [16].

Although pyrimorph is currently in use to control various fungal pathogens [15–17], its functional mechanism has remained unclear. The presence of a common CAA moiety has led to the suggestion that pyrimorph may work in a fashion similar to that of other CAA-type fungicides [18]. One CAA member, mandipropamid, was shown to target the pathway of cell wall synthesis by inhibiting the CesA3 cellulose synthases [19]. However, treatment of fungal pathogens with pyrimorph appeared to affect multiple cellular pathways, including, but not limited to, those of cellular energy metabolism and cell wall biosynthesis, either directly or indirectly [20]. Indeed, a recent report has correlated the pyrimorph resistance phenotype in *P. capsici* with mutations in the CesA3 gene [21].

Other mechanisms of pyrimorph action have yet to be investigated. In particular, its potential interference with cellular respiratory chain components leading to reduced ATP synthesis appears to be a reasonable hypothesis for the observed inhibitory effects on energy demanding processes such as mycelial growth and cytospor germination of fungi. Here, we report the effects of pyrimorph on electron flow through the isolated fungal mitochondrial respiratory chain and the identification of the cyt *bc*<sub>1</sub> complex as pyrimorph's primary target. Kinetic experiments suggest that the mode of pyrimorph inhibition is to interfere with substrate access to the ubiquinol oxidation site but in a way that differs from other *bc*<sub>1</sub> inhibitors, suggesting a novel mode of inhibitory mechanism.

## Materials and Methods

The pyrimorph used in all experiments was synthesized in our laboratory. Dimethomorph was a gift from Jiangshu Frey Chemical Co. Ltd. (Jiangshu Province, China). Cyt *c* (from horse heart, type III) was purchased from Sigma-Aldrich (St. Louis, MI). 2,3-dimethoxy-5-methyl-6-(10-bromodecyl)-1,4-benzoquinol (Q<sub>0</sub>C<sub>10</sub>BrH<sub>2</sub>) was prepared as previously reported [22]. N-dodecyl-β-D-maltoside (β-DDM) and N-octyl-β-D-glucoside (β-OG) were purchased from Affymetrix (Santa Clara, CA). All other chemicals were purchased and are of the highest grade possible.

### Preparation of Light Mitochondria from *Phytophthora capsici*

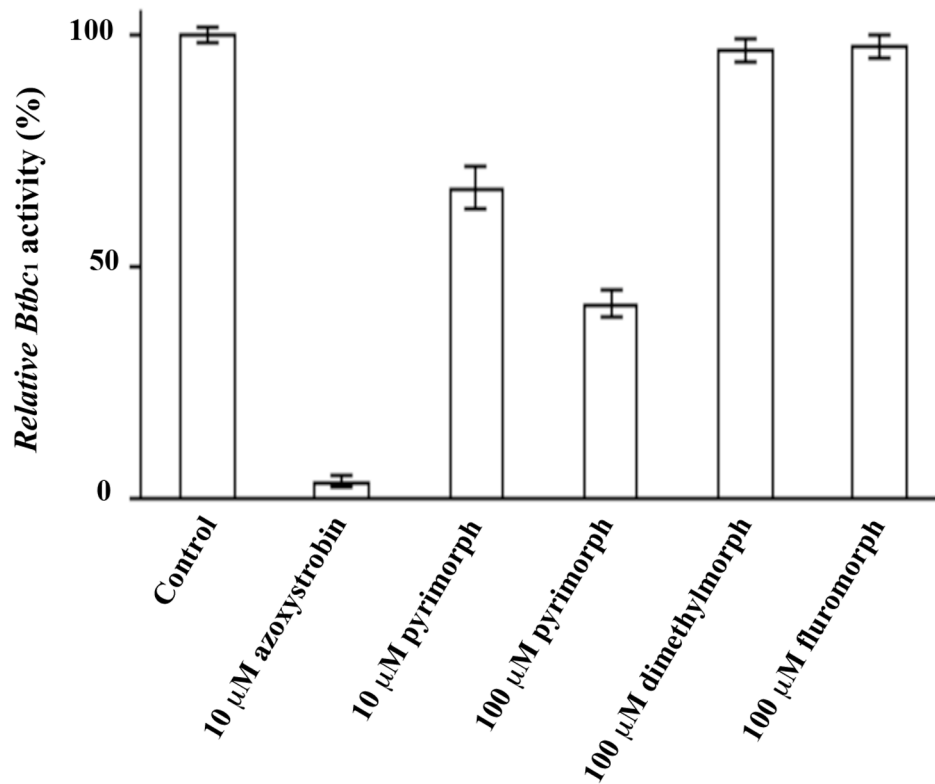
Light mitochondrial fraction were prepared from cultured mycelia from laboratory strain *Phytophthora capsici* *Leonia* (*P. capsici*), which was grown in CA liquid medium (8% carrot juice and 2% glucose) for 5 days in the dark at 25°C [23]. 10 g mycelia (fresh weight) were washed with 0.6 M mannitol solution and ground up for 5 minutes with an ice-cold mortar and pestle in 100 ml buffer A containing 10 mM MOPS•KOH, pH 7.1, 0.3 M mannitol, 1 mM EDTA and 0.1% (w/v) bovine serum albumin (BSA) and 30 g of sea sand. The homogenate was centrifuged at 3,200×g for 10 min at 4°C and the supernatant was further centrifuged at 12,000×g for 30 min. The precipitate, light mitochondrial fraction, was resuspended and washed with 20 ml buffer B containing 10 mM MOPS•KOH, pH 7.1, 0.25 M sucrose and 1 mM EDTA and pelleted again by centrifugation at 12,000×g for 20 min at 4°C. The mitochondrial preparation was resuspended in buffer A and the protein concentration was adjusted to 0.1 mg/ml.

**Table 1.** Inhibition of respiratory complexes I, II, and III by pyrimorph.

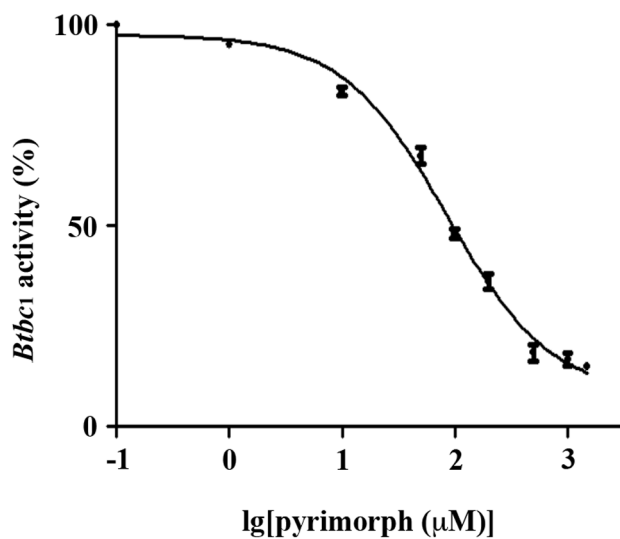
Complex	Concentration of pyrimorph (μM)					
	0	4	8	12	16	
I (Inhibition of NADH oxidation)	51.8±2	52.7±3	48.3±6	52.1±7	49.8±1	3.8
II (Inhibition of DCPIP reduction)	112.7	83.6±4	58.3±6	25.1±7	6.8±1	94.6
III (Inhibition of cyt <i>c</i> reduction)	27.24	1.29±1	–	–	–	–

\*Millimolar extinction coefficients for oxidation NADH is 6.2 mM<sup>-1</sup> cm<sup>-1</sup> [49], for DCPIP is 21 mM<sup>-1</sup> cm<sup>-1</sup> [50], and for cyt *c* is 18.5 mM<sup>-1</sup> cm<sup>-1</sup> [24].  
doi:10.1371/journal.pone.0093765.t001

A



B



C

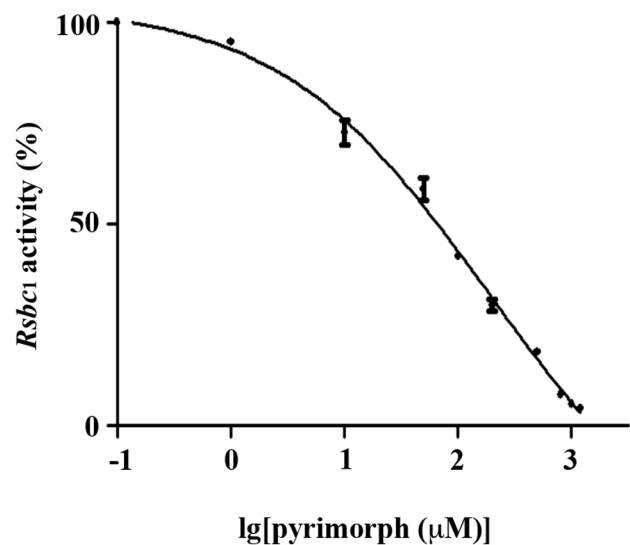


**Figure 1. Inhibition of cyt  $bc_1$  by various inhibitors.** (A) Inhibition of *Btbc*<sub>1</sub> by several amide fungicides and azoxystrobin at indicated concentrations. The control is the activity of *bc*<sub>1</sub> in the absence of inhibitor, which is set to 100%. (B) Concentration-dependent inhibition of *Btbc*<sub>1</sub> by pyrimorph. (C) Concentration-dependent inhibition of *Rsbc*<sub>1</sub> by pyrimorph. doi:10.1371/journal.pone.0093765.g001

#### Inhibition of the ET Activity of *P. capsici* Mitochondria by Pyrimorph

The activities of mitochondrial respiratory chain components were assayed using the Mitochondria Complex Activity Assay Kit (Genmed Scientifics, Inc. USA, Wilmington, DE) following manufacturer's instruction. Briefly, Complex I activity was

measured by following the oxidation of NADH by monitoring the decrease in absorbance difference between 340 nm and 380 nm. The reaction mixture (1 ml) consisted of 50 mM potassium phosphate buffer, pH 7.6, 0.25 mM NADH and 50 mM decylubiquinone as the electron acceptor. Crude mitochondria (200  $\mu$ g protein) were added to start the reaction.

Complex II activity was estimated as the rate of reduction of ubiquinone to ubiquinol by succinate, which can be followed by the secondary reduction of 2,6-dichlorophenolindophenol (DCPIP) as the ubiquinol forms. The reaction mixture (1 ml) contained 50 mM potassium phosphate buffer, pH 7.6, 20 mM succinate, 1.0 mM EDTA, 0.05 mM DCPIP and 3 mM NaN<sub>3</sub>, and 50 mM decylubiquinone. Crude mitochondria (65 µg) were added to initiate the reaction and the decrease in absorbance at 600 nm was followed as DCPIP becomes reduced. Complex III activity was assayed by following the increase in absorbance at 550 nm as cyt *c* becomes reduced using decylubiquinol as an electron donor. Here, the reaction mixture (1 ml) consisted of 50 mM potassium phosphate buffer, pH 7.6, 0.1% BSA, 0.1 mM EDTA, 60 mM oxidized cyt *c*, and 150 µM decylubiquinol. Crude mitochondria (10 µg protein) were then added to initiate the reaction.

### Purification of Cyt *bc*<sub>1</sub> Complexes from Beef Heart and Photosynthetic Bacterium *Rhodobacter sphaeroides*

Bovine heart mitochondrial *bc*<sub>1</sub> (*Btbc*<sub>1</sub>) complex was prepared starting from highly purified succinate-cyt *c* reductase, as previously reported [24]. The *bc*<sub>1</sub> particles were solubilized by deoxycholate and contaminants were removed by a 15-step ammonium acetate fractionation. The purified *bc*<sub>1</sub> complex was recovered in the oxidized state from the precipitates formed between 18.5% and 33.5% ammonium acetate saturation. The final product was dissolved in 50 mM Tris•HCl buffer, pH 7.8, containing 0.66 M sucrose resulting in a stock solution with a protein concentration of 30 mg/ml, which was stored at -80°C. The concentrations of cyt *b* and *c*<sub>1</sub> were determined spectroscopically using millimolar extinction coefficients of 28.5 and 17.5 mM<sup>-1</sup> cm<sup>-1</sup> for cyt *b* and *c*<sub>1</sub>, respectively.

To prepare cyt *bc*<sub>1</sub> complex from the photosynthetic bacterium *R. sphaeroides* (*Rsb*<sub>1</sub>), *R. sphaeroides* strain BC17 cells bearing the pRKD418-*fb*cbFBC<sub>6H</sub>Q plasmid [25] were grown photosynthetically at 30°C in an enriched Sistrom medium containing 5 mM glutamate and 0.2% casamino acids [26]. The growth was monitored by measuring the OD<sub>600</sub> value every 3–5 h. Cells were transferred to a larger batch or harvested when OD<sub>600</sub> reached 1.8–2.0. Chromatophore membranes were prepared from BC17 cells as described previously [27] and stored at a very high concentration in the presence of 20% glycerol at -80°C. To purify the hexahistidine-tagged *Rsb*<sub>1</sub> complex, the freshly prepared chromatophores or frozen chromatophores thawed on ice were adjusted to a cyt *b* concentration of 25 µM with a solubilization buffer containing 50 mM Tris•HCl, pH 8.0 at 4°C, and 1 mM MgSO<sub>4</sub>. 10% (w/v) β-DDM was added to the chromatophore suspension to a final concentration of 0.56 mg detergent/nmole of cyt *b* followed by addition of 4M NaCl solution to a final concentration of 0.1 M. After stirring on ice for 1 hour, the admixture was centrifuged at 220,000×g for 90 minutes; the supernatant was collected and diluted with equal volume of the solubilization buffer followed by passing through a Ni-NTA agarose column (100 nmole of cyt *b*/ml of resin) pre-equilibrated with two volumes of the solubilization buffer. After loading, the column was washed sequentially with the following buffers until the absence of greenish color in effluent was reached: washing buffer (50 mM Tris•HCl, pH 8.0 at 4°C, containing 100 mM NaCl) +0.01% β-DDM; washing buffer +0.01% β-DDM and 5 mM histidine; washing buffer +0.5% β-OG; washing buffer +0.5% β-OG and 5 mM histidine. The cyt *bc*<sub>1</sub> complex was eluted with the washing buffer +0.5% β-OG and 200 mM histidine. Pure fractions were combined and concentrated by Centriprep-30

concentrator. Glycerol was added to a final concentration of 10% before storage at -80°C.

### Measurement of *bc*<sub>1</sub> Activity and its Inhibition (IC<sub>50</sub>) by Various Inhibitors

The activities of isolated cyt *bc*<sub>1</sub> complexes were assayed following the reduction of substrate cyt *c*. The purified *bc*<sub>1</sub> complexes were diluted to a final concentration of 0.1 µM and 1 µM based on the concentration of cyt *b* for *Btbc*<sub>1</sub> and *Rsb*<sub>1</sub>, respectively, in the B200 buffer (50mM Tris•HCl, pH 8.0, 0.01% β-DDM, 200 mM NaCl). The assay mixture contains 100 mM phosphate buffer, pH 7.4, 0.3 mM EDTA, and 80 µM cyt *c*, and Q<sub>0</sub>C<sub>10</sub>BrH<sub>2</sub> at a final concentration of 5 µM. The addition of 3 µl of diluted *bc*<sub>1</sub> solution initiates the reaction, which is recorded immediately following the cyt *c* reduction at 550 nm wavelength for 100 seconds in a two-beam Shimadzu UV-2250 PC spectrophotometer at 23°C. The amount of cyt *c* reduced over a given period of time was calculated using a millimolar extinction coefficient of 18.5 mM<sup>-1</sup> cm<sup>-1</sup>.

To measure the effect of *bc*<sub>1</sub> inhibitors, *bc*<sub>1</sub> was pre-incubated at various concentrations of an inhibitor for 15 minutes prior to the measurement of its activity. The IC<sub>50</sub> value was calculated by a least-squares procedure fitting the equation  $(Y = A_{\min} + (A_{\max} - A_{\min}) / (1 + 10^{(X - \log IC_{50})}))$  implemented in the commercial package Prism, where A<sub>max</sub> and A<sub>min</sub> are maximal and minimal activities, respectively. Although the chemical properties of Q<sub>0</sub>C<sub>10</sub>BrH<sub>2</sub> are comparable to those of Q<sub>0</sub>C<sub>10</sub>H<sub>2</sub>, the former is a better substrate for the cyt *bc*<sub>1</sub> complex isolated in detergent solution [22].

### Reaction Kinetics of *bc*<sub>1</sub> in the Presence of Inhibitors

To measure the enzyme kinetics of cyt *bc*<sub>1</sub> complex under inhibitory conditions, purified cyt *bc*<sub>1</sub>, either *Btbc*<sub>1</sub> or *Rsb*<sub>1</sub>, was assayed at different concentrations of substrates. When the Q<sub>0</sub>C<sub>10</sub>BrH<sub>2</sub> concentration was varied (1 µM, 2 µM, 5 µM, 10 µM, 20 µM) the cyt *c* concentration was kept constant at 80 µM, whereas when the concentration of cyt *c* varied (1 µM, 2 µM, 4 µM, 8 µM, 12 µM, 16 µM) the Q<sub>0</sub>C<sub>10</sub>BrH<sub>2</sub> concentration was kept constant at 50 µM. The reactions were initiated by adding 3 µl of diluted *bc*<sub>1</sub> solution (0.1 µM for *Btbc*<sub>1</sub> or 1.0 µM for *Rsb*<sub>1</sub>) pre-incubated with various concentrations of inhibitors for 15 minutes. The time course of the absorbance change due to cyt *c* reduction was recorded continuously at 550 nm. Initial rates were determined from the slopes in the linear portion of cyt *c*<sub>1</sub> reduction time course.

### Analysis of Cyt *bc*<sub>1</sub> Spectra in the Presence of Inhibitors

For each run a solution of 1 ml bovine cyt *bc*<sub>1</sub> at a cyt *b* concentration of 5 µM was fully reduced with addition of a tiny amount of sodium dithionite and its spectrum was obtained in the range of 520–600 nm. A specific inhibitor was added at various concentrations to the reduced *bc*<sub>1</sub> complex and was scanned repeatedly until no changes were observed. All scans were stored digitally and difference spectra were produced by subtracting the corresponding spectrum of the inhibitor-free, fully reduced *bc*<sub>1</sub> complex.

### Measurement of Cyt *b* and *c*<sub>1</sub> Reduction Time Course in a Single Turnover Reaction

The enzyme was diluted to a final concentration of about 4 µM of cyt *c*<sub>1</sub> in 1 ml of B200 buffer (50 mM Tris•HCl, pH 8.0, 0.01% β-DDM, 200 mM NaCl) and oxidized fully by adding a tiny amount of potassium ferricyanide. The spectrum of the fully oxidized enzyme in the range of 520–590 nm was stored.

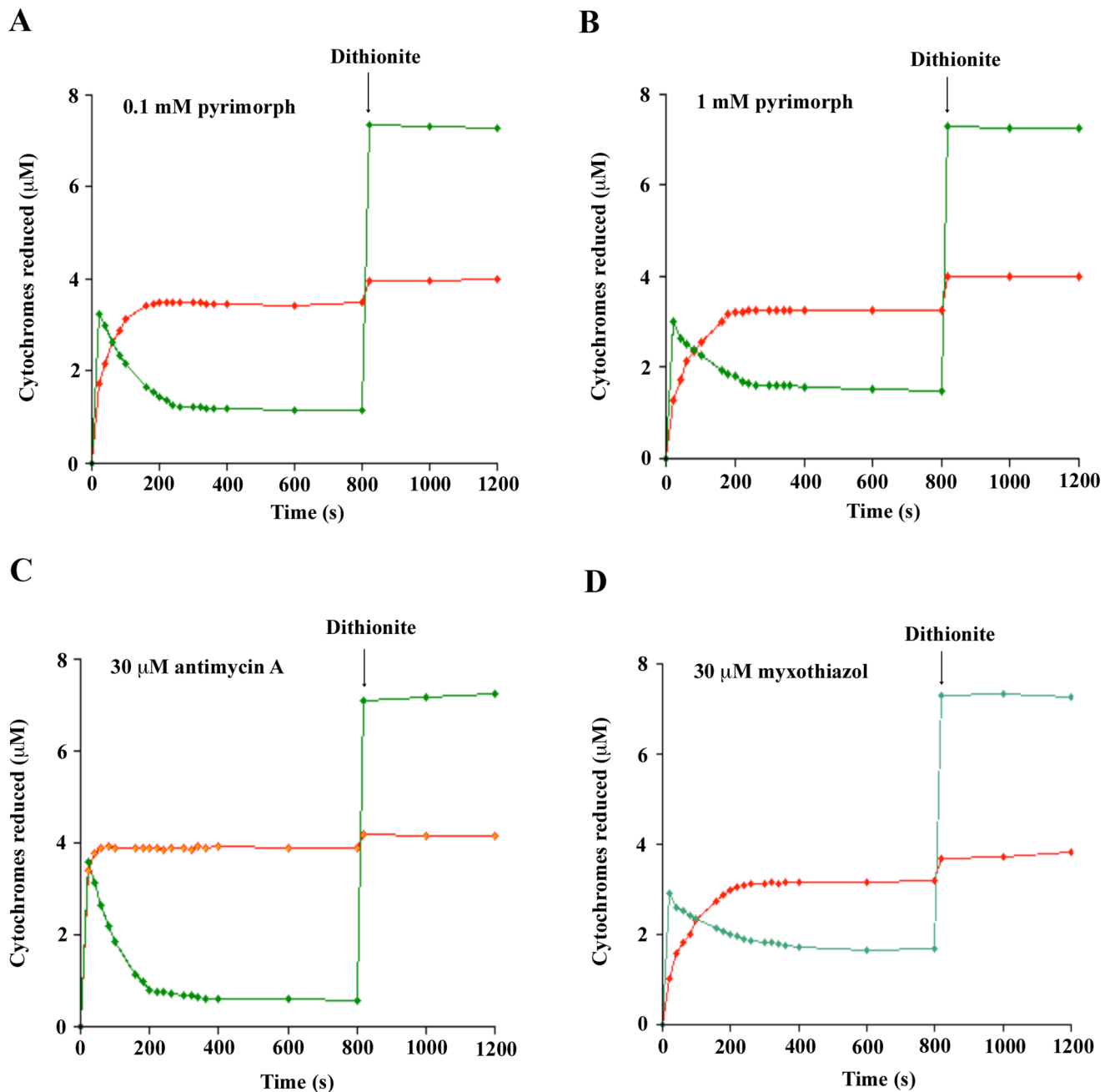


**Figure 2. Influences of cyt *b* and *c*<sub>1</sub> reduction by pyrimorph.** Isolated *Btbc*<sub>1</sub> was incubated with indicated inhibitors followed by single turnover reaction initiated by addition of 10 μM Q<sub>0</sub>C<sub>10</sub>BrH<sub>2</sub>. The spectra were recorded immediately following the mixing and every 20 seconds thereafter. At the 800 second time point, a tiny amount of sodium dithionite was added to reduce both cyt *b* and *c*<sub>1</sub>. The amounts of reduced cyt *b* and *c*<sub>1</sub> were calculated and plotted as a function of time. The green trace is the amount of cyt *b* reduced over time and the red one is the amount of cyt *c*<sub>1</sub> reduced. (A) 100 μM pyrimorph, (B) 1000 μM pyrimorph, (C) 30 μM myxothiazol, and (D) 30 μM antimycin A. doi:10.1371/journal.pone.0093765.g002

Inhibitors at various concentrations were introduced and incubated for 2 min followed by addition of the ubiquinol analog Q<sub>0</sub>C<sub>10</sub>BrH<sub>2</sub> to a final concentration of 10 μM to start the reaction. Spectra were recorded at 20-second intervals starting immediately after mixing. After 800 seconds the enzyme was fully reduced by dithionite. The spectrum of the fully oxidized complex was subtracted from that at each time point and the amounts of reduced cyt *c*<sub>1</sub> and *b* at a given time were calculated from the difference spectra at 552–540 nm and 560–576 nm, respectively.

### Molecular Docking of Pyrimorph to Cyt *b*

Coordinates for the receptor molecule were taken from the protein data bank (pdb) entry 1SQX, for the stigmatellin inhibited complex of *Btbc*<sub>1</sub>. The side chains of residues E271 and F274 were modeled as standard rotamers consistent with their positions in apo *Btbc*<sub>1</sub>. The ligand molecule, pyrimorph, was drawn and converted to a SMILES string using tools from the CADD Group [28]. The SMILES string was converted by the program Elbow [29] to 3D coordinates and energy minimized in GAMESS [30].

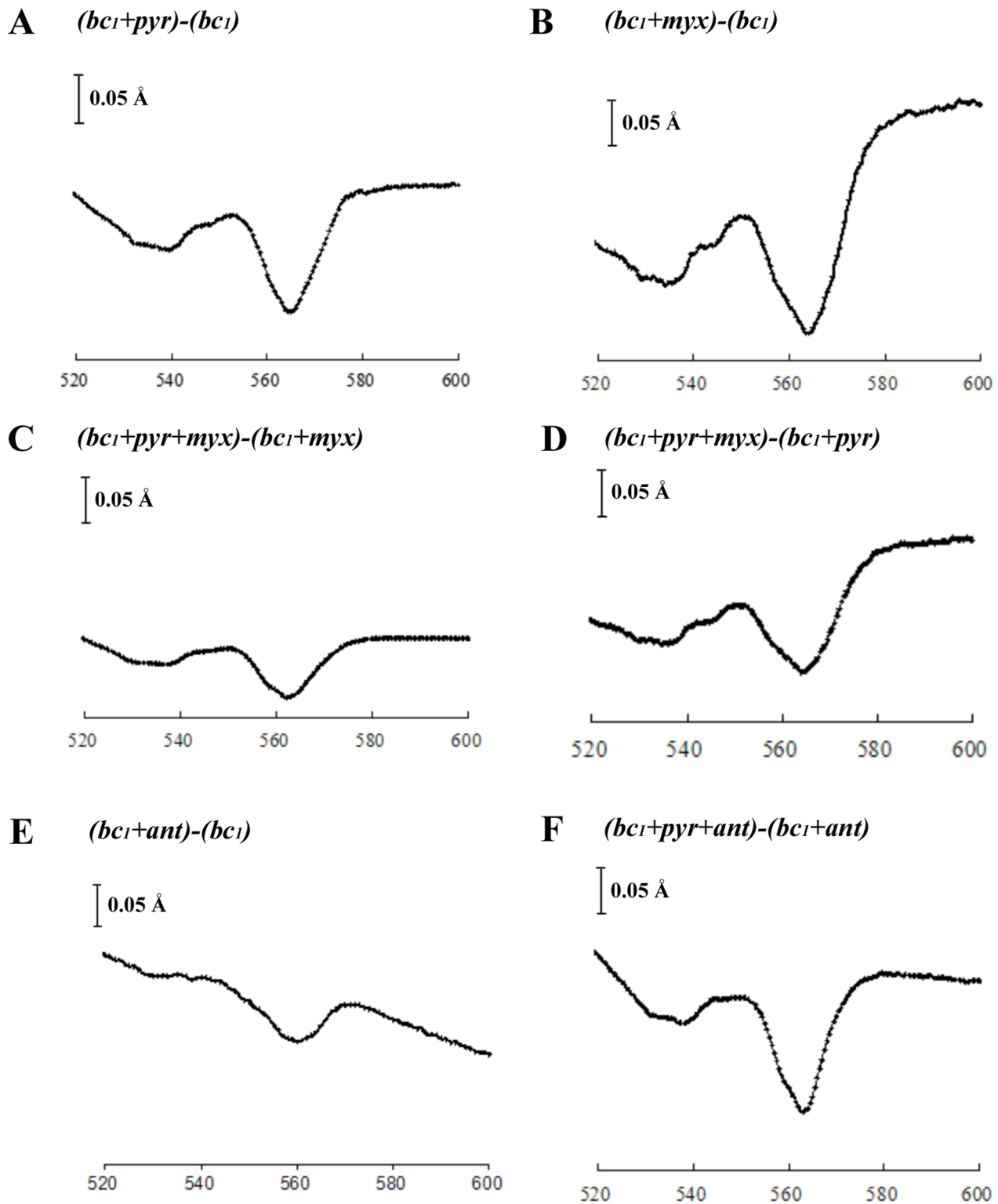


**Figure 3. Difference spectra of inhibitors and inhibitors combinations to reduced  $Btbc_1$ .** All spectra were recorded with purified  $Btbc_1$  at a concentration of 5  $\mu$ M of cyt  $b$  with the concentrations of inhibitor as indicated. Prior to spectral scan, the  $bc_1$  complex was reduced by addition of dithionite. (A) Spectrum of reduced  $Btbc_1$  in the presence of 1 mM pyrimorph (pyr) minus that of reduced  $Btbc_1$  alone. (B) Spectrum of reduced  $Btbc_1$  in the presence of 10  $\mu$ M myxothiazol (myx) minus that of reduced  $Btbc_1$  alone. (C) and (D) The spectrum of reduced  $Btbc_1$  in equilibration with 1 mM pyrimorph followed by addition of 10  $\mu$ M myxothiazol minus spectrum of reduced  $Btbc_1$  in the presence of 10  $\mu$ M myxothiazol or 1 mM pyrimorph, respectively. (E) Spectrum of reduced  $Btbc_1$  in the presence of 10  $\mu$ M antimycin A (ant) minus spectrum of reduced  $Btbc_1$  alone. (F) Spectrum of reduced  $Btbc_1$  after equilibration with 1 mM pyrimorph and 10  $\mu$ M antimycin A in sequence minus spectrum of reduced  $Btbc_1$  in the presence of antimycin A.

doi:10.1371/journal.pone.0093765.g003

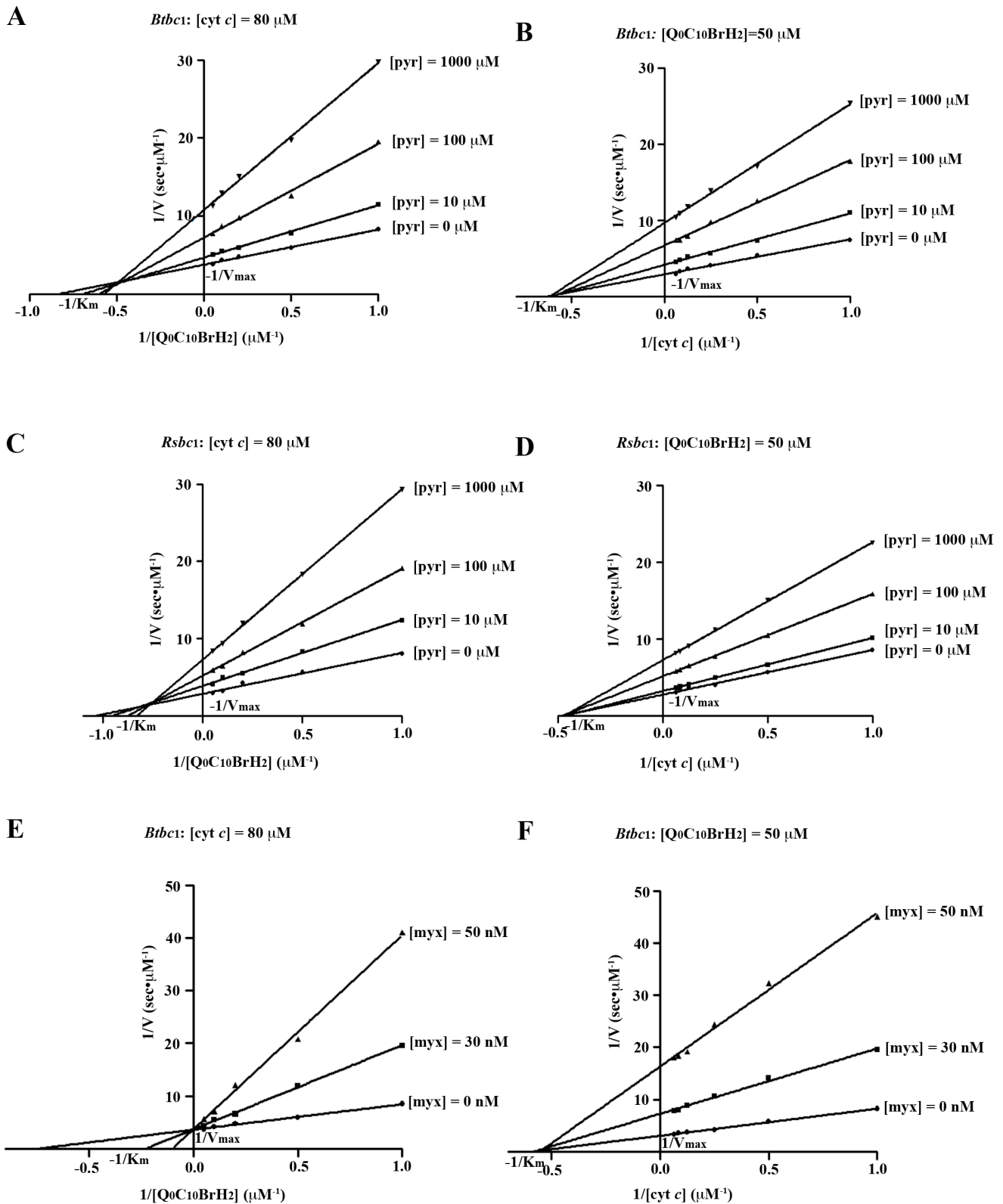


**Figure 4. Double-reciprocal (Lineweaver-Burk) plots for  $bc_1$  inhibition.** Four different concentrations of 0, 10, 100 and 1000  $\mu\text{M}$  were used for pyrimorph and three, 0, 30 and 50 nM were used for myxothiazol. Each point represents a mean value of at least 3 independent experimental measurements. (A) Inhibition of *Btbc1* by pyrimorph with variations in concentration of Q<sub>0</sub>C<sub>10</sub>BrH<sub>2</sub>. (B) Inhibition of *Btbc1* by pyrimorph with variations in concentration of cyt  $c$ . (C) Inhibition of *Rsbcl* by pyrimorph with variations in concentration of Q<sub>0</sub>C<sub>10</sub>BrH<sub>2</sub>. (D) Inhibition of *Rsbcl* by pyrimorph with variations in concentration of cyt  $c$ . (E) Inhibition of *Btbc1* by myxothiazol with variations in concentration of Q<sub>0</sub>C<sub>10</sub>BrH<sub>2</sub>. (F) Inhibition of *Btbc1* by myxothiazol with variations in concentration of cyt  $c$ . doi:10.1371/journal.pone.0093765.g004

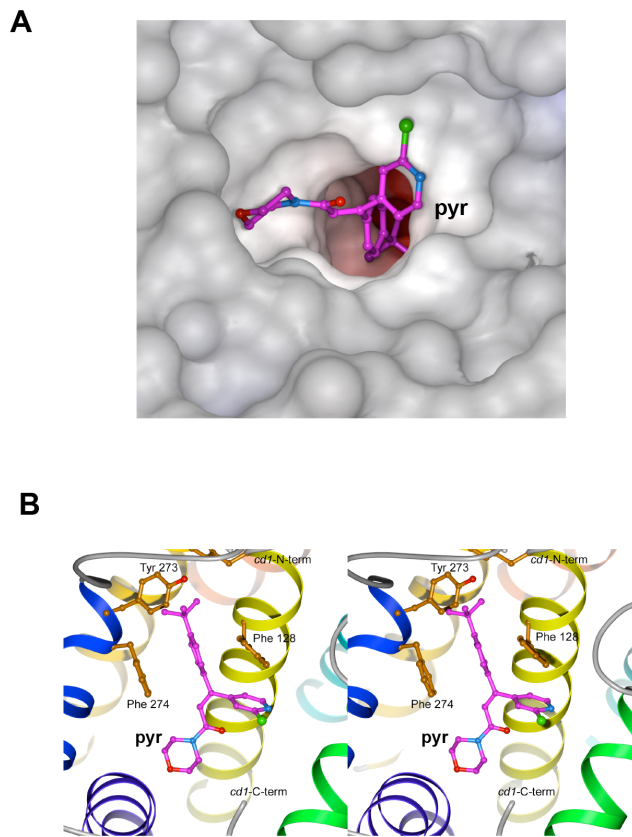


**Figure 5. Molecular docking showing the possible binding site and interaction of pyrimorph in the cyt *b* subunit.** (A) Molecular surface of the cyt *b* subunit is given, showing the access portal leading to the Q<sub>P</sub> site, which is blocked by the docked pyrimorph in a ball-and-stick model with atoms of carbon in magenta, nitrogen in blue, oxygen in red and chlorine in green. (B) Stereoscopic pair showing the detailed interactions between residues in the cyt *b* subunit with the docked pyrimorph molecule.

doi:10.1371/journal.pone.0093765.g005

Both receptor and ligand molecules were converted to standard pdbqt files using mglttools [31]. For all docking runs, the acrylamide moiety (C7 = C8–C9 = O16) of pyrimorph was fixed in the *syn-periplanar* conformation because the alternative *anti*-conformation would bring the larger morpholino and pyridyl groups into close contact.

Two approaches to docking were taken: (1) as the most likely binding sites for inhibitors are the Q<sub>P</sub> and the Q<sub>N</sub> sites, docking attempts were made first at those known sites. (2) In a second set of runs, no prior knowledge of sites was imposed but the program Q-site-finder [32] was used to locate all potential binding sites and docking was carried out at all sensible locations. Docking pyrimorph to known and unknown inhibitor binding sites was performed using the program Autodock Vina [33].

## Results

### Pyrimorph Blocks the Mitochondrial Respiratory Chain by Targeting cyt *bc*<sub>1</sub> Complex

To test whether pyrimorph inhibits fungal growth by interfering with the cellular energy metabolism pathway, in particular the mitochondrial respiratory chain, we isolated light mitochondrial fraction from the pathogenic fungus *P. capsici* and examined the ability of pyrimorph to inhibit various segments of the respiratory

chain (Table 1). It is quite clear that pyrimorph has no effect on the activity of Complex I, as a concentration of pyrimorph as high as 16 μM was unable to inhibit NADH oxidation catalyzed by Complex I. By contrast, under the same conditions, pyrimorph inhibits 94.6% of Complex II activity. Most importantly, Complex III, the cyt *bc*<sub>1</sub> complex, shows the highest sensitivity toward pyrimorph, with 95.3% inhibition even at 4 μM concentration.

Although the effects of pyrimorph on the mitochondrial respiratory chain of *P. capsici* were clearly demonstrated, such effects could be indirect. To ascertain that the target of pyrimorph is indeed the cyt *bc*<sub>1</sub> complex, we used highly purified cyt *bc*<sub>1</sub> from beef heart (*Bos taurus bc*<sub>1</sub> or *Btbc*<sub>1</sub>) and assayed inhibition of its cyt *c* reductase activity by pyrimorph. The result was compared to the well-known anti-*bc*<sub>1</sub> fungicide azoxystrobin and two other CAA-type fungicides, dimethomorph and flumorph. As shown in Fig. 1A, *Btbc*<sub>1</sub> activities are reduced to 67% and 42% of the control, respectively, in the presence of 10 μM and 100 μM of pyrimorph. Azoxystrobin is able to inhibit *bc*<sub>1</sub> activity by more than 95% at 10 μM concentration. However, the two CAA-type fungicides, dimethomorph and flumorph, displayed no activity at all against *Btbc*<sub>1</sub>. These results indicated that pyrimorph is different from other members of CAA-type fungicides and more importantly established that pyrimorph is indeed an inhibitor of the cyt *bc*<sub>1</sub> complex, albeit a weak one.

We subsequently determined 50% inhibitory concentration (IC<sub>50</sub>) for pyrimorph against isolated cyt *bc*<sub>1</sub> complexes from both bovine mitochondria and photosynthetic bacterium *R. sphaeroides* (*Rsb*<sub>1</sub>). Pyrimorph is slightly more potent against *Rsb*<sub>1</sub>, giving an IC<sub>50</sub> value of 69.2 μM; it gives an IC<sub>50</sub> of 85.0 μM for *Btbc*<sub>1</sub> (Figs. 1B and 1C). As a comparison, the well-known *bc*<sub>1</sub> inhibitor stigmatellin and azoxystrobin give IC<sub>50</sub> values of 2.8 nM and 47.7 nM, respectively, for isolated *Btbc*<sub>1</sub> by our measurement (data not shown) under the same assay conditions. Since *Rsb*<sub>1</sub> has only four subunits, it is therefore certain that pyrimorph targets the essential subunits of the *bc*<sub>1</sub> complex.

### Effect of Pyrimorph Binding on Reduction of the Cyt *b* and *c*<sub>1</sub> by Ubiquinol

Nearly all cyt *bc*<sub>1</sub> inhibitors bind to the Q<sub>N</sub> site, Q<sub>P</sub> site or both [34]. It is known that binding of inhibitors produces various effects on spectra of cyt *b* and *c*<sub>1</sub> heme groups, as well as on redox potential and conformation of the iron-sulfur protein [34–38]. These effects ultimately determine the rate and amount of cyt *b* or *c*<sub>1</sub> reduced under equilibrium conditions and can be exploited to compare modes of action of different inhibitors [39], distinguishing for example a Q<sub>N</sub> site inhibitor from a Q<sub>P</sub> site one. Starting with a completely oxidized enzyme, *Btbc*<sub>1</sub> was mixed with substrate Q<sub>0</sub>C<sub>10</sub>BrH<sub>2</sub> in the presence of pyrimorph at two different concentrations (0.1 mM and 1.0 mM); no cyt *c* was used as the terminal electron acceptor. The amount of cyt *b* including *b*<sub>L</sub> and *b*<sub>H</sub> hemes and cyt *c*<sub>1</sub> reduced as a function of time was recorded (Figs. 2A and 2B). The results were compared with those produced by Q<sub>N</sub> site inhibitor antimycin A (Fig. 2C) and by Q<sub>P</sub> site inhibitor myxothiazol (Fig. 2D).

In the absence of the high-potential electron acceptor cyt *c*, only a single enzymatic turnover at the Q<sub>P</sub> site is possible when the Q<sub>N</sub> site inhibitor antimycin A is bound. Under such conditions, both cyt *b* and *c*<sub>1</sub> were rapidly reduced reaching maximal reduction of nearly half of the *b*-type hemes and all of the *c*-type heme perhaps even before the first measurement was recorded (Fig. 2C). Once reaching maximal reduction, cyt *b* began non-enzymatic oxidation rather rapidly, whereas the redox state of cyt *c*<sub>1</sub> remained unchanged. When the Q<sub>P</sub> site is occupied by an inhibitor such as myxothiazol, not a single turnover is possible (Fig. 2D). The

initial rapid reduction of cyt  $b$  was most likely via the reverse reaction at the  $Q_N$  site and cyt  $c_1$  reduction was entirely non-enzymatic. Thus, the rate of cyt  $c_1$  reduction and that of cyt  $b$  re-oxidation can be employed to determine which site an inhibitor targets.

Clearly, the reduction behavior of cytochromes  $b$  and  $c_1$  induced by pyrimorph distinguishes it from that induced by antimycin A (Figs. 2A, 2B and 2C), demonstrating that pyrimorph does not target the  $Q_N$  site. By contrast, the time courses of cyt  $b$  and  $c_1$  reduction in the presence of pyrimorph or myxothiazol resemble each other (Figs. 2A, 2B, and 2D), except that the latter inhibitor takes a longer time for cyt  $c_1$  to be maximally reduced than pyrimorph does. This result puts pyrimorph into the category of a  $Q_P$ -site inhibitor by either directly or indirectly competing with ubiquinol for the  $Q_P$  site.

### Spectral Analyses Suggest the Binding of Pyrimorph near $Q_P$ Site

Single turnover experiments suggested that pyrimorph acts in a fashion similar to that of  $Q_P$  site inhibitors. It was thus necessary to determine how pyrimorph interferes with  $bc_1$  function at the  $Q_P$  site. Since spectral changes, especially red shifts in the  $\alpha$ - and  $\beta$ -band caused by binding of inhibitors to reduced  $bc_1$ , were successfully used to deduce information about their binding interactions [37,40], a similar approach was taken for pyrimorph. By comparing the spectra of reduced  $bc_1$  bound with pyrimorph to those obtained with known  $Q_P$  or  $Q_N$  site inhibitors such as myxothiazol or antimycin A, we hoped to gain insight into the binding interactions and location.

Binding of pyrimorph causes the spectrum to red shift, as the difference spectrum  $[(bc_1+pyr)-bc_1]$  shows a trough centered around 565 nm (Fig. 3A), which is an indication that binding of pyrimorph affects cyt  $b$  hemes. This spectrum was compared to spectra with bound  $Q_P$  site inhibitor myxothiazol  $[(bc_1+myx)-bc_1]$  and  $Q_N$  site inhibitor antimycin A  $[(bc_1+ant)-bc_1]$ , respectively (Figs. 3B and 3E). At a first glance, it seems that the spectral change due to pyrimorph binding resembles that caused by myxothiazol binding, despite considerable differences (see below), indicating that pyrimorph binds closer to the  $b_L$  heme or the  $Q_P$  site. Indeed, binding pyrimorph to  $bc_1$  does not seem to interfere with subsequent binding of antimycin A, as the difference spectrum of  $[(bc_1+pyr+ant) - (bc_1+ant)]$  (Fig. 3F) looks almost identical to  $[(bc_1+pyr)-(bc_1)]$  (Fig. 3A). This experiment confirms that pyrimorph does not target the  $Q_N$  site.

However, binding of pyrimorph to  $bc_1$  does affect subsequent binding of myxothiazol and *vice versa*, because the difference spectrum  $[(bc_1+pyr+myx) - (bc_1+myx)]$  (Fig. 3C) does not look like that of  $[(bc_1+pyr)-(bc_1)]$  (Fig. 3A), nor does the difference spectrum  $[(bc_1+pyr+myx) - (bc_1+pyr)]$  (Fig. 3D) resemble that of  $[(bc_1+myx)-(bc_1)]$  (Fig. 3B). These spectra indicate the possibility that both inhibitors can co-exist near the  $Q_P$  pocket and influence each other. Since the binding of myxothiazol to the  $Q_P$  pocket is well established, the experiment further suggests that pyrimorph may have a different binding mode from that of myxothiazol.

### Inhibitory Kinetics of Cyt $bc_1$ Suggests the Mode of Pyrimorph Action

The possibility that pyrimorph has a different mode of action is of particular interest in light of our extensive knowledge on the development of resistance to existing inhibitors. To further probe the mechanism of pyrimorph's action, we investigated the kinetic properties of  $bc_1$  function under pseudo first-order reaction conditions by measuring its activity with respect to changes in

concentration of either substrates  $Q_0C_{10}BrH_2$  or cyt  $c$  in the presence of different amount of pyrimorph, allowing double reciprocal or Lineweaver-Burk plots to reveal the relationship between  $1/V$  and  $1/[S]$ . The measurements were done for both  $Btbc_1$  and  $Rsb_1$ , revealing nearly identical kinetic behavior (Fig. 4). As shown in Figs. 4A and 4C, in the presence of a constant 80  $\mu M$  cyt  $c$  and with increasing concentrations of  $Q_0C_{10}BrH_2$ , both  $K_m$  and  $V_{max}$  are altered as is the  $K_m/V_{max}$  ratio. Expectedly, as the concentration of pyrimorph increases, the  $V_{max}$  decreases; at a constant pyrimorph concentration, the reciprocal enzyme activity  $1/V$  has a positive slope with respect to  $1/[S]$ . However, the  $K_m$  value for the substrate quinol changed, falling between competitive (Fig. 4E) and non-competitive (Fig. 4F) inhibitions. Thus, pyrimorph falls into the category of a mixed-type, noncompetitive inhibitor with respect to the substrate ubiquinol, suggesting that it competes, both directly and indirectly, with ubiquinol to occupy the  $Q_P$  site.

At a constant 50  $\mu M$   $Q_0C_{10}BrH_2$  concentration and with varying concentrations of cyt  $c$ , double-reciprocal plots show that x-intercepts remain the same with or without pyrimorph (Figs. 4B and 4D), suggesting that the apparent  $K_m$  for substrate cyt  $c$  remains unchanged. Thus, pyrimorph is a noncompetitive inhibitor with respect to cyt  $c$ . As a control, we performed the same experiments with  $Btbc_1$  using the classic  $Q_P$ -site inhibitor myxothiazol, showing that myxothiazol is a competitive inhibitor for the substrate quinol but a non-competitive inhibitor for cyt  $c$  (Figs. 4E and 4F).

### Docking of Pyrimorph to cyt $b$ Subunit

Docking of pyrimorph to known inhibitor-binding sites in the cyt  $b$  subunit of  $Btbc_1$  were performed with Autodock Vina and resulted in top solutions at the  $Q_P$  site with a binding free energy of  $-9.7$  kcal/mol and  $-9.2$  kcal/mol at the  $Q_N$  site, representing a 2.3-fold difference in binding affinity between the two sites. These energy values can be compared with binding of other known  $bc_1$  inhibitors such as stigmatellin, giving rise to a binding free energy of  $-10.5$  kcal/mol. Potential inhibitor binding sites outside the known active sites were searched by  $Q$ -site-finder and the top 20 sites suggested (which included the  $Q_P$  and  $Q_N$  site) were subjected to extensive docking trials using Autodock Vina but no new locations showing improved affinity over the classic sites were identified. The  $Q_P$  site showed the highest binding affinity to pyrimorph. Unlike traditional inhibitors, pyrimorph does not enter the  $Q_P$  site, but rather blocks the entrance or portal to the quinol oxidation site (Fig. 5A). While its morpholino and 4-(2-chloro pyridyl) moieties stay in the central cavity of the  $bc_1$  dimer, its 4-(*tert*-butyl) phenyl group enters the access portal, where it is stabilized by the aromatic side chain of F274 and partially by F128. The latter primarily interacts with the pyridyl moiety via aromatic-aromatic (Ar-Ar) interactions. The *tert*-butyl group that penetrates into the  $Q_P$  site is flanked by the residues Y273, Y131 and P270, establishing beneficial van-der-Waals contacts.

### Discussion

Resistance to cyt  $bc_1$  inhibitors has been extensively investigated, revealing a wide variety of underlying mechanisms including target site mutations [41,42], activation of alternative oxidase pathways [43,44], altered metabolic degradation [45], reduced uptake and increased efflux [46,47]. By far, target site mutation is the most prevalent form of resistance that develops against  $bc_1$  inhibitors. Thus, extensive research has been focusing on how to overcome resistance caused by target site mutations. Finding

inhibitors that target alternative sites seems to be an attractive strategy.

### Pyrimorph is a Multi-target Fungicide Displaying Inhibitory Activity against Cyt *bc*<sub>1</sub>

Pyrimorph is a fungicide containing a carboxylic acid amide (CAA) moiety and was shown to be cross-resistant with other CAA fungicides such as mandipropamid, dimethomorph and flumorph [21], suggesting the possibility that pyrimorph may function in a manner similar to that of other CAA-type fungicides such as mandipropamid for which the mode of action was established by inhibiting cellulose synthase 3 or CesA3 [19]. In a recent publication [21], pyrimorph-resistant isolates of *P. capsici* were selected in the presence of the inhibitor and the three most resistant strains share a common mutation (Q1077K) in the CesA3 gene, which is different from the one (G1104V) selected for mandipropamid resistance [19]. However, it remains to be seen whether transfer of the resistant allele to the sensitive parental strain would make the latter pyrimorph-resistant. So far there is no direct evidence from *in vitro* biochemical experiments that shows at the protein level the inhibition of CesA3 by pyrimorph.

In the current study, we followed up on the previous observation that pyrimorph may act on the cellular respiratory chain of pathogenic fungi [20]. We showed that pyrimorph is able to suppress the respiratory chain function at 4  $\mu$ M concentration by inhibiting the activity of Complex III in isolated mitochondria of *P. capsici* mycelia (Table 1). We further showed conclusively that pyrimorph inhibits purified mitochondrial as well as bacterial *bc*<sub>1</sub> complexes with IC<sub>50</sub> values at sub-millimolar range (Fig. 1). By contrast, two other CAA-type inhibitors, dimethomorph and flumorph, displayed no inhibitory activity against *bc*<sub>1</sub> complex (Fig. 1A).

It did not escape our notice that cyt *bc*<sub>1</sub> in light mitochondrial fraction isolated from *P. capsici* mycelia appears to be more sensitive to pyrimorph than purified bovine or bacterial *bc*<sub>1</sub> complexes, suggesting the following possibilities: (1) Direct comparison between results of two very different assays is not a fair comparison, because in isolated light mitochondrial fraction the estimation of cyt *bc*<sub>1</sub> concentration is difficult in the presence of many different proteins. However, the inhibitory concentrations or IC values are directly related to the amount of enzyme in the assay solution. So the lower IC value could be due to a lower concentration of *bc*<sub>1</sub> in the assay conditions. (2) Being a hydrophobic compound, pyrimorph may preferentially partition into the lipid bilayer of mitochondrial membranes, leading to a higher local concentration and in turn to the apparent 95% inhibition at 4  $\mu$ M concentration (Table 1, Fig. 1). (3) Conversely, the presence of detergent (micelles) in the solution of purified *bc*<sub>1</sub> complex might lower the effective concentration of pyrimorph. This scenario is less likely, as the concentration of  $\beta$ -DDM in our assay buffer is barely above one critical micelle concentration (CMC). (4) The cyt *bc*<sub>1</sub> of *P. capsici* is more sensitive to pyrimorph than either bovine or bacterial *bc*<sub>1</sub>. However, we note that the purified bacterial complex is more sensitive to pyrimorph than bovine *bc*<sub>1</sub> but only by a factor of 1.2. The difference might simply be a reflection of changes in the sequences and we do observe that bacterial *bc*<sub>1</sub> exhibits slightly higher similarity to fungal than bovine mitochondrial cyt *b*.

### Pyrimorph Likely Acts Near but not at the Q<sub>P</sub> Site

The fact that pyrimorph inhibits both 11-subunit *Btbc*<sub>1</sub> and 4-subunit *Rsb*<sub>1</sub> demonstrates that the inhibitor acts on cyt *b*, cyt *c*<sub>1</sub> or ISP subunits of the complex; it does not inhibit mitochondrial *bc*<sub>1</sub> function through binding to the so-called supernumerary subunits

(Figs. 1B and 1C). The two potential sites for pyrimorph binding are Q<sub>N</sub> and Q<sub>P</sub> in the cyt *b* subunit and so far all experimental evidence suggests a binding site near the Q<sub>P</sub> site: (1) Single turnover experiments show the reduction rate of cyt *c*<sub>1</sub> and re-oxidation rate of cyt *b* in the presence of two different concentrations of pyrimorph (Figs. 2A and 2B) are very similar to those in the presence of the Q<sub>P</sub> site inhibitor myxothiazol (Fig. 2D), but are drastically different from those in the presence of the Q<sub>N</sub> site inhibitor antimycin A (Fig. 2C). (2) Difference spectra of reduced cyt *bc*<sub>1</sub> also provided strong evidence that pyrimorph targets the Q<sub>P</sub> site (Fig. 3), because the difference spectrum of [(*bc*<sub>1</sub>+pyr)-(bc<sub>1</sub>)] (Fig. 3A) resembles that of [(*bc*<sub>1</sub>+myx)-(bc<sub>1</sub>)] (Fig. 3B) but not that of [(*bc*<sub>1</sub>+ant)-(bc<sub>1</sub>)] (Fig. 3E).

While the analysis of the difference spectra points to the Q<sub>P</sub> pocket as the target site, it also suggests that pyrimorph has a non-overlapping binding site with the classic Q<sub>P</sub> site inhibitor myxothiazol (Fig. 3). Indeed, double-reciprocal or Lineweaver-Burk plots of *bc*<sub>1</sub> activity showed that pyrimorph acts as a mixed-type, non-competitive inhibitor with respect to the substrate ubiquinol (Figs. 4A and 4C), suggesting that pyrimorph may act both competitively and non-competitively for the substrate ubiquinol (Fig. 4E). Mechanistically, it means that pyrimorph is capable of modulating the binding of the substrate ubiquinol without directly competing with it at the active site, which categorizes it as a mixed-type, non-competitive inhibitor [48].

Unlike classic Q<sub>P</sub> site inhibitors that compete directly with substrate ubiquinol for interactions with the same set of residues in the Q<sub>P</sub> site, pyrimorph rather seems to block the portal to the Q<sub>P</sub> site, through which the substrate ubiquinol has to pass to contact ISP. Simultaneously, a good portion of pyrimorph is held outside the substrate-binding pocket by hydrophobic forces. Consequently, ubiquinol has to actively displace pyrimorph from the entrance in order to gain access to the Q<sub>P</sub> site as in the case of a competitive inhibitor. On the other hand, as pyrimorph has the ability to adhere well to the lipophilic sides of the portal that leads to the Q<sub>P</sub> site of cyt *b*, it may stay close and possibly interfere with the necessary motion of the cd1/cd2 helix and with the release of ubiquinone, displaying inhibitory activities more characteristic of non-competitive inhibitors. This picture is entirely consistent with biochemical and spectral characterizations of pyrimorph, qualifying it as a mixed-type, non-competitive inhibitor.

Molecular modeling of other CAA-type fungicides such as dimethomorph indicate a very similar binding position and orientation to the Q<sub>P</sub> site but with a significantly lower free energy for binding, consistent with the observation that both dimethomorph and flumorph are not *bc*<sub>1</sub> inhibitors (Fig. 1A). Since both dimethomorph and flumorph structurally resemble pyrimorph, it is clear that the shape of pyrimorph is not a dominant factor for its ability to bind *bc*<sub>1</sub>. At the very least the binding of pyrimorph has sparked ideas for a dual approach to inhibitor design: (1) on the side that binds to the Q<sub>P</sub> entrance, modifications could significantly increase the affinity, making it a better competitive inhibitor. (2) Improvements in hydrophobicity or geometric factors on the side that stays outside the Q<sub>P</sub> pocket, the inhibitor could enhance its non-competitive properties. Should it be possible to design a dual type inhibitor, fungal resistance may be stalled for an extended period. Suggestions for improvements might include modifications of the *tert*-butyl group to include polar groups (hydroxy methyl, methoxy methyl, etc.) that are within the reach of E271 (both sidechain and backbone amide) as well as sterically demanding aromatic groups that may take advantage of the large, aromatic cavity of the Q<sub>P</sub> site. On the side that stays outside of the Q<sub>P</sub> pocket, variations of saturated and aromatic ring systems seem likely to improve binding properties, as it appears

that the morpholino group and the chloro-pyridyl group can change places with minimal change in binding energy.

## Acknowledgments

We thank George Leiman for editorial assistance during the preparation of this manuscript. This study utilized the high-performance computational capabilities of the Biowulf Linux cluster at the National Institutes of Health, Bethesda, MD (<http://biowulf.nih.gov>).

## References

1. Trumpower BL (1990) Cytochrome *bc*<sub>1</sub> complexes of microorganisms. *Microbiological Reviews* 54: 101–129.
2. Keilin D (1925) On cytochrome, a respiratory pigment, common to animals, yeast, and higher plants. *Proc R Soc Lond B98*: 312–399.
3. Leadbeater A (2012) Resistance risk to QoI fungicides and anti-resistance strategies. In: Thind TS, editor. *Fungicide resistance in crop protection: risk and management*. CAB eBooks. 141–152.
4. Trumpower BL (1990) The protonmotive Q cycle. Energy transduction by coupling of proton translocation to electron transfer by the cytochrome *bc*<sub>1</sub> complex. *Journal of Biological Chemistry* 265: 11409–11412.
5. Mitchell P (1975) Protonmotive redox mechanism of the cytochrome *b-c*<sub>1</sub> complex in the respiratory chain: protonmotive ubiquinone cycle. *FEBS Lett* 56: 1–6.
6. Xia D, Yu CA, Kim H, Xia JZ, Kachurin AM, et al. (1997) Crystal structure of the cytochrome *bc*<sub>1</sub> complex from bovine heart mitochondria. *Science* 277: 60–66.
7. Iwata S, Lee JW, Okada K, Lee JK, Iwata M, et al. (1998) Complete structure of the 11-subunit bovine mitochondrial cytochrome *bc*<sub>1</sub> complex [see comments]. *Science* 281: 64–71.
8. Zhang Z, Huang L, Shulmeister VM, Chi YI, Kim KK, et al. (1998) Electron transfer by domain movement in cytochrome *bc*<sub>1</sub>. *Nature* 392: 677–684.
9. Hunte C, Koepke J, Lange C, Rossmannith T, Michel H (2000) Structure at 2.3 Å resolution of the dimeric cytochrome *bc*<sub>1</sub> complex from the yeast *Saccharomyces cerevisiae* co-crystallized with an antibody Fv fragment. *Structure* 15: 669–684.
10. Esser L, Elberry M, Zhou F, Yu CA, Yu L, et al. (2008) Inhibitor complexed structures of the cytochrome *bc*<sub>1</sub> from the photosynthetic bacterium *Rhodospirillum rubrum* at 2.40 Å resolution. *J Biol Chem* 283: 2846–2857.
11. Kleinschroth T, Castellani M, Trinh CH, Morgner N, Brutschy B, et al. (2011) X-ray structure of the dimeric cytochrome *bc*<sub>1</sub> complex from the soil bacterium *Paracoccus denitrificans* at 2.7-Å resolution. *Biochim Biophys Acta* 1807: 1606–1615.
12. Berry EA, Huang L, Saechao LK, Pon NG, Valkova-Valchanova M, et al. (2004) X-ray structure of *Rhodospirillum rubrum* cytochrome *bc*<sub>1</sub>: comparison with its mitochondrial and chloroplast counterparts. *Photosynthesis Research* 81: 251–275.
13. Esser L, Yu CA, Xia D (2013) Structural Basis of Resistance to Anti-Cytochrome *bc*<sub>1</sub> Complex Inhibitors: Implication for Drug Improvement. *Curr Pharm Des*.
14. Mu CW, Yuan HZ, Li N, Fu B, Xiao YM, et al. (2007) Synthesis and fungicidal activities of a novel series of 4-[3-(pyrid-4-yl)-3-substituted phenyl acryloyl] morpholine. *Chem J Chinese U* 28: 1902–1906.
15. Chen XX, Yuan HZ, Qin ZH, Qi SH, Sun LP (2007) Preliminary studies on antifungal activity of pyrimorph. *Chinese Journal of Pesticide Science* 9: 229–234.
16. Wang HC, Sun HY, Stammler G, Ma JX, Zhou MG (2009) Baseline and differential sensitivity of *Peronospora litchii* (lychee downy blight) to three carboxylic acid amide fungicides. *Plant Pathology*.
17. Du YN, Wang GZ, Li G (2008) Preventive and therapeutic experiment of 20% Bimalin on phytophthora blight of Capsicum. *Modern Agrochemicals* 7: 44–46.
18. Sun H, Wang H, Stammler G, Ma J, Zhou MG (2010) Baseline Sensitivity of Populations of *Phytophthora capsici* from China to Three Carboxylic Acid Amide (CAA) Fungicides and Sequence Analysis of Cholinephosphotransferases from a CAA-sensitive Isolate and CAA-resistant Laboratory Mutants. *Journal of Phytopathology* 158: 244–252.
19. Blum M, Boehler M, Randall E, Young V, Csukai M, et al. (2010) Mandipropamid targets the cellulose synthase-like PiCesA3 to inhibit cell wall biosynthesis in the oomycete plant pathogen, *Phytophthora infestans*. *Mol Plant Pathol* 11: 227–243.
20. Yan X, Qin W, Sun L, Qi S, Yang D, et al. (2010) Study of inhibitory effects and action mechanism of the novel fungicide pyrimorph against *Phytophthora capsici*. *J Agric Food Chem* 58: 2720–2725.
21. Pang Z, Shao J, Chen L, Lu X, Hu J, et al. (2013) Resistance to the novel fungicide pyrimorph in *Phytophthora capsici*: risk assessment and detection of point mutations in CcsA3 that confer resistance. *PLoS One* 8: e56513.
22. Yu CA, Yu L (1982) Syntheses of biologically active ubiquinone derivatives. *Biochemistry* 21: 4096–4101.
23. Mitani S, Araki S, Takii Y, Ohshima T, Matsuo N, et al. (2001) The biochemical mode of action of the novel selective fungicide cyazofamid: specific inhibition of mitochondrial complex III in *Phytophthora infestans*. *Pesticide Biochemistry and Physiology* 71: 107–115.
24. Yu L, Yang S, Yin Y, Cen X, Zhou F, et al. (2009) Chapter 25 Analysis of electron transfer and superoxide generation in the cytochrome *bc*<sub>1</sub> complex. *Methods Enzymol* 456: 459–473.
25. Mather MW, Yu L, Yu CA (1995) The involvement of threonine 160 of cytochrome *b* of *Rhodospirillum rubrum* cytochrome *bc*<sub>1</sub> complex in quinone binding and interaction with subunit IV. *Journal of Biological Chemistry* 270: 28668–28675.
26. Tian H, Yu L, Mather MW, Yu CA (1997) The Involvement of Serine 175 and Alanine 185 of Cytochrome *b* of *Rhodospirillum rubrum* Cytochrome *bc*<sub>1</sub> Complex in Interaction with Iron-Sulfur Protein. *Journal of Biological Chemistry* 272: 23722–23728.
27. Yu L, Yu CA (1991) Essentiality of the molecular weight 15,000 protein (subunit IV) in the cytochrome *b-c*<sub>1</sub> complex of *Rhodospirillum rubrum*. *Biochemistry* 30: 4934–4939.
28. Nicklaus M.C SM (2012) CADD Group Cheminformatics Tools and User Services.
29. Adams PD, Afonine PV, Bunkoczi G, Chen VB, Davis IW, et al. (2010) PHENIX: a comprehensive Python-based system for macromolecular structure solution. *Acta Crystallographica Section D* 66: 213–221.
30. Schmidt MW, Baldrige KK, Boatz JA, Elbert ST, Gordon MS, et al. (1993) General Atomic and Molecular Electronic-Structure System. *Journal of Computational Chemistry* 14: 1347–1363.
31. Sanner MF (1999) Python: A programming language for software integration and development. *Journal of Molecular Graphics and Modelling* 17: 57–61.
32. Laurie AT, Jackson RM (2005) Q-SiteFinder: an energy-based method for the prediction of protein-ligand binding sites. *Bioinformatics* 21: 1908–1916.
33. Trott O, Olson AJ (2010) AutoDock Vina: Improving the speed and accuracy of docking with a new scoring function, efficient optimization, and multithreading. *Journal of Computational Chemistry* 31: 455–461.
34. Esser L, Quinn B, Li Y, Zhang M, Elberry M, et al. (2004) Crystallographic studies of quinol oxidation site inhibitors: A modified classification of inhibitors for the cytochrome *bc*<sub>1</sub> complex. *Journal of Molecular Biology* 341: 281–302.
35. von Jagow G, Link TA (1986) Use of specific inhibitors on the mitochondrial *bc*<sub>1</sub> complex. *Methods in Enzymology* 126: 253–271.
36. Link TA, Haase U, Brandt U, von Jagow G (1993) What information do inhibitors provide about the structure of the hydroquinone oxidation site of ubiquinol: cytochrome *c* oxidoreductase? *Journal of Bioenergetics and Biomembrane* 25: 221–232.
37. von Jagow G, Liungdahl PO, Craff P, Ohnishi T, Trumpower BL (1984) An Inhibitor of Mitochondrial Respiration Which Binds to Cytochrome *b* and Displaces Quinone from the Iron-Sulfur Protein of the Cytochrome *bc*<sub>1</sub> Complex. *Journal of Biological Chemistry* 259: 6318–6326.
38. von Jagow G, Engel WD (1981) Complete inhibition of electron transfer from ubiquinol to cytochrome *b* by teh combined action of antimycin and myxothiazol. *FEBS Letters* 136: 19–24.
39. Berry EA, Huang LS, Lee DW, Daldal F, Nagai K, et al. (2010) Ascochlorin is a novel, specific inhibitor of the mitochondrial cytochrome *bc*<sub>1</sub> complex. *Biochim Biophys Acta* 1797: 360–370.
40. Jordan DB, Livingston RS, Bisaha JJ, Duncan KE, Pember SO, et al. (1999) Mode of action of famoxadone. *Pesticide Science* 55: 105–118.
41. Bolgunas S, Clark DA, Hanna WS, Mauvais PA, Pember SO (2006) Potent inhibitors of the Q<sub>i</sub> site of the mitochondrial respiration complex III. *J Med Chem* 49: 4762–4766.
42. Bresseur G, Saribas AS, Daldal F (1996) A compilation of mutations located in the cytochrome *b* subunit of the bacterial and mitochondrial *bc*<sub>1</sub> complex. *BiochimBiophysActa* 1275: 61–69.
43. Wood PM, Hollomon DW (2003) A critical evaluation of the role of alternative oxidase in the performance of strobilurin and related fungicides acting at the Q<sub>o</sub> site of complex III. *Pest Manag Sci* 59: 499–511.
44. Steinfeld U, Sierotzki H, Parisi S, Gisi U (2001) Sensitivity of mitochondrial respiration to different inhibitors in *Venturia inaequalis*. *Pesticide Management Science* 57: 787–796.
45. Dosnon-Olette R, Schroder P, Bartha B, Aziz A, Couderchet M, et al. (2011) Enzymatic basis for fungicide removal by *Elodea canadensis*. *Environ Sci Pollut Res Int* 18: 1015–1021.
46. Gaur M, Choudhury D, Prasad R (2005) Complete inventory of ABC proteins in human pathogenic yeast, *Candida albicans*. *J Mol Microbiol Biotechnol* 9: 3–15.
47. Hill P, Kessl J, Fisher N, Meshnick S, Trumpower BL, et al. (2003) Recapitulation in *Saccharomyces cerevisiae* of cytochrome *b* mutations

## Author Contributions

Conceived and designed the experiments: YMX ZHQ DX. Performed the experiments: YMX LE FZ CL YHZ DX. Analyzed the data: YMX LE DX. Contributed reagents/materials/analysis tools: CAY. Wrote the paper: YMX LE DX.

- conferring resistance to atovaquone in *Pneumocystis jiroveci*. *Antimicrob Agents Chemother* 47: 2725–2731.
48. Garrett RH, Grisham CM (1999) *Biochemistry*. Fort Worth, Philadelphia, San Diego, New York, Orlando, Austin, San Antonio, Toronto, Montreal, London, Sydney, Tokyo: Saunders College Publishing, Harcourt Brace College Publishers.
49. Yoshida T, Murai M, Abe M, Ichimaru N, Harada T, et al. (2007) Crucial structural factors and mode of action of polyene amides as inhibitors for mitochondrial NADH-ubiquinone oxidoreductase (complex I). *Biochemistry* 46: 10365–10372.
50. Hatefi Y, Stiggall DL (1978) Preparation and properties of succinate: ubiquinone oxidoreductase (complex II). *Methods Enzymol* 53: 21–27.